Available online at www.sciencedirect.com
ScienceDirect
Journal of Chromatography B, 855 (2007) 2–13
JOURNAL OF CHROMATOGRAPHY B
www.elsevier.com/locate/chromb

Review

Tandem time-of-flight (TOF/TOF) mass spectrometry and the curved-field reflectron☆

Robert J. Cotter*, Wendell Griffith, Christine Jelinek

Middle Atlantic Mass Spectrometry Laboratory, Johns Hopkins University School of Medicine, Baltimore, MD 21205, United States

Received 22 September 2006; accepted 4 January 2007
Available online 13 January 2007

Abstract

The *curved-field reflectron* (CFR), when used as the second mass analyzer in a tandem time-of-flight mass spectrometer, provides a design that enables the use of very high energy *collision-induced dissociation* (CID). Specifically, this is because the wide energy bandwidth of the CFR obviates the need for floating the collision region to decelerate the precursor ions and subsequently reaccelerating product ions to enable reflectron focusing. Here we describe the evolution of tandem instruments based on the CFR, from its introduction in 1993 to the current commercial TOF^2 mass spectrometer from Shimadzu Corporation, and briefly review the history of TOF/TOF instruments. A number of applications are also described. One is the characterization of a C-terminal cleavage of cystatin C that appears to be associated with patients with remitting relapse multiple sclerosis (RRMS). Both *surface-enhanced laser desorption/ionization* (SELDI) and MALDI were used on a high performance TOF instrument operating in the MS and MS/MS modes. Tandem TOF mass spectrometry has also been used to determine the acetylation sites on histones and on the enzyme, *histone acetyl transferase* (HAT), responsible for the modification. Acetylation has been determined quantitatively for multiple sites on histone H3 and H4 using a deuteroacetylation method. For a number of closely spaced sites on the histone tail regions, MS/MS enables us to then determine both the order and distribution of acetylation.

Keywords: Tandem mass spectrometry; Time-of-flight; Curved-field reflectron; Matrix-assisted laser desorption/ionization (MALDI); Surface-enhanced laser desorption/ionization (SELDI); Multiple sclerosis; Cystatin; Histone acetyl transferase (HAT); Histones; Acetylation

Contents

1. What is the "curved-field reflectron"?

The IUPAC Mass Spectrometry Terms and Definitions project defines the curved-field reflectron as: a reflectron in which the retarding field is non-linear. The voltages on the lens elements follow the equation of an arc of a circle according to $R^2 = V^2 + x^2$, where x is the distance from the reflectron entrance,

☆ This paper was presented at the 31st Annual Meeting of the Japanese Society for Biomedical Mass Spectrometry, Nagoya, Japan, 28–29 September 2006.

* Corresponding author. Tel.: +1 410 955 3022; fax: +1 410 955 3420.
E-mail address: rcotter@jhmi.edu (R.J. Cotter).

1570-0232/$ – see front matter © 2007 Elsevier B.V. All rights reserved.
doi:10.1016/j.jchromb.2007.01.009

V the voltage and R is a constant [1]. The CFR is in fact identical in construction to the single-stage reflectron, except for the imposition of the non-linear voltages on the lenses. The CFR was introduced and developed by Cotter and Cornish [2] specifically for its ability to focus product ions in a tandem mass spectrometer.

A reflectron is a time-of-flight mass analyzer that compensates for the kinetic energy spread of ions from the source by reflecting the ions back along the same flight path prior to detection. The reflectron was introduced in 1973 by Mamyrin et al. [3] to improve mass resolution, and the simplest embodiment is the *single-stage* reflectron shown in Fig. 1a [4]. Here the average flight time of an ion of mass m and kinetic energy eV is:

$$t = \left(\frac{m}{2eV}\right)^{1/2}[L_1 + L_2 + 4d] \tag{1}$$

where L_1 and L_2 are the drift regions that the ions traverse in the forward and reverse directions, d the *average penetration depth* into the reflecting field and V is the ion accelerating voltage. The reflectron is generally designed such that $L_1 + L_2 = 4d$, so that ions spend an equal amount of time in the drift and reflecting field regions. When an ion has excess kinetic energy: $eV + U_0$, the time spent in the drift regions:

$$t = \left(\frac{m}{2(eV + U_0)}\right)^{1/2}[L_1 + L_2] \tag{2}$$

will be less, as the ion will be traveling faster. However, the penetration depth for this faster ion will increase:

$$d' = \frac{eV + U_0}{eV}d \tag{3}$$

so that it spends more time in the reflecting field. Solving the equation:

$$t = \left(\frac{m}{2(eV + U_0)}\right)^{1/2}\left[L_1 + L_2 + \left(\frac{eV + U_0}{eV}\right)4d\right] \tag{4}$$

for an ion with excess energy, requires expansion of the term $(eV + U_0)$ about eV assuming that U_0 is very small with respect to eV, where only a first-order solution is possible. Second-order solutions are possible using a dual-stage reflectron (Fig. 1b), and in fact, the reflectron first introduced by Mamyrin et al. was a dual-stage reflectron [3]. The dual stage reflectron utilizes two retarding field regions, generally separated by a grid. The first region is generally short, with a high retarding field, while the second is longer with a shallower field. Fig. 2a and b compare the retarding voltage versus depth profile for the single- and dual-stage reflectrons, respectively. In either case, the reflectron provides kinetic energy focusing when the energy spread ΔU_0 is small. In a 20 keV instrument, this might be in the range of 100 eV to 1 keV.

It is of course possible to design a reflectron with perfect (that is: infinite-order) focusing. Mamyrin describes a quadratic reflectron [5] in which the voltages placed on the lens elements

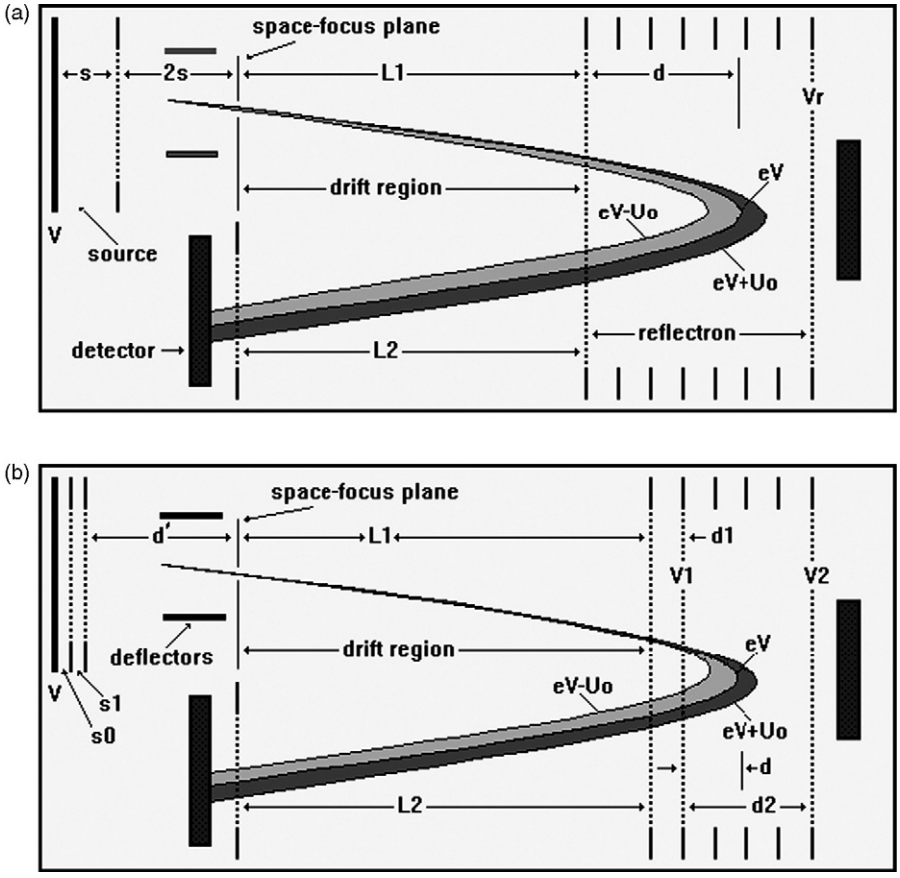

Fig. 1. Schematic of a single-stage (a) and a dual stage (b) reflectron. Reprinted with permission from ref. [4].

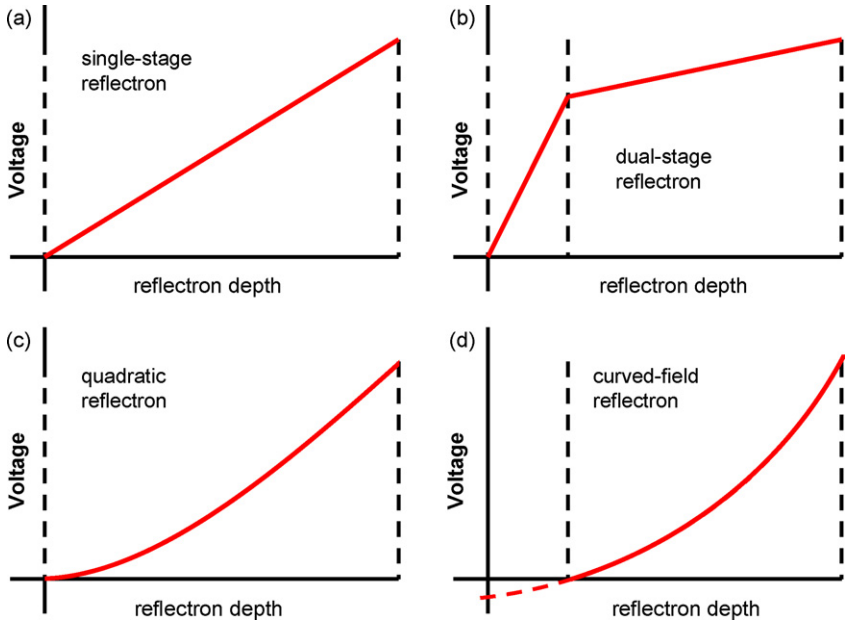

Fig. 2. Dependence of the potential on distance from the entrance grid for (a) a single-stage reflectron, (b) a dual-stage reflectron, (c) a quadratic reflectron and (d) the curved-field reflectron. The dashed vertical lines illustrate the positions of the ion transmission grids.

is: $V_x = ax^2$, where x is the distance from the entrance to the reflectron and a is a constant. The voltage versus depth profile of the quadratic reflectron is shown in Fig. 2c. The flight time of an ion m in a quadratic reflectron:

$$t = 2\int_0^{x_{\max}} \frac{\mathrm{d}x}{2e/m(V_x - ax^2)} = \pi\left(\frac{m}{2ea}\right)^{1/2} \quad (5)$$

depends only on mass and is independent of energy. While it would appear that this is a perfect reflectron, it should be noted that it is difficult to achieve a quadratic potential using a series of lens elements as the potential along to the center line tends to "flatten out", even while the potential along the edges of the reflectron is quadratic. One consequence of this field shape is that the ion beam becomes divergent and ion transmission is reduced. To some degree this problem is mitigated by using a "narrow bore" design in which the reflectron depth is very much greater than the radius.

A unique property of the quadratic reflectron is that it does not include linear regions (i.e. L_1 and L_2) or compensate for differences in the time spent in them. Similarly, it does not compensate for differences that ions spend in the ion source, as these ions (initially with different energies) arrive at the reflectron at slightly different times. However, because product ions formed by fragmentation after the source (in the drift regions or collision chambers) have a range of kinetic energies well outside that which can be focused by single or dual-stage reflectrons, the quadratic reflectron is an obvious choice for the second stage of a tandem mass spectrometer. A recent example of this is the tandem TOF instrument designed by Giannakopoulos et al. [6].

The *curved-field reflectron* has some similarities to the quadratic reflectron, specifically a non-linear field, but was developed to address several practical problems associated with ion transmission and product ion formation. The *arc-of-a-circle* potential shown in Fig. 2d is considerably shallower than the quadratic potential (and indeed very close to the linear potential or constant field case) to improve ion transmission. In addition, the potential does not approach ground asymptotically; rather there is a discontinuity at the entrance grid, similar to the single and dual-stage reflectrons. Also, the reflectron includes and accommodates a drift region. In a tandem TOF instrument, a drift region following the collision chamber will permit focusing of ions that fragment less than promptly, that is: after leaving the collision chamber.

2. Tandem TOF/TOF configurations

In double-focusing and tandem sector mass spectrometers, product ions are formed by fragmentation in a field-free region. These product ions not only have a different mass m_b than that of their precursors m_a, but also have a different kinetic energy:

$$E_b = \frac{m_b}{m_a} eV \quad (6)$$

where V is the accelerating voltage. Thus, in sector instruments, it was necessary to compensate for this change in energy by a linked scan of the magnetic (B) and electrostatic (E) fields. In a TOF instrument, fragmentation in the field-free (drift) region produces product ions with different masses, different kinetic energies, but the same velocities as their precursors. Because they have the same velocities, they also have the same flight times and cannot be distinguished in a simple linear time-of-flight instrument. Their flight times can be distinguished, however, if the ions encounter an electric field. Thus, the simplest form of a tandem (or TOF/TOF) mass spectrometer has a (retarding or accelerating) voltage step. An example (Table 1) is the instru-

Table 1
History of tandem TOF configurations

Year	Type	Description	Reference
1989	TOF/RTOF	Linear mass analyzer with an orthogonal reflectron mass analyzer	Schey et al. [8]
1992	TOF/TOF	Two in-line linear mass analyzers with a voltage step	Jardine et al. [7]
1992	TOF/RTOF	MS1 is second-order space focus. Ions are reaccelerated into a second-order reflectron	Boesl et al. [9]
1993	RTOF/RTOF	ArF excimer photodissociation in floated chamber between two reflectron analyzers	Seeterlin et al. [10]
1993	RTOF/RTOF	Pulsed gas, floated collision chamber between two dual-stage reflectrons	Cotter and Cornish [11]
1993	RTOF/RTOF	CID in floated collision region with two single-stage reflectrons	Cornish and Cotter [12]
1994	RTOF/RTOF	Single stage as MS1; curved-field reflectron (CFR) as MS2	Cornish and Cotter [2]
2002	TOF/RTOF	MS2 is a quadratic reflectron	Giannakopoulos et al. [6]

ment designed in 1992 by Jardine et al. [7]. However, a retarding or accelerating field will introduce a spread in ion flight times, so that it makes sense to utilize a reflectron to distinguish product and precursor ion flight times while focusing these ions at the same time. The difficulty is again shown in Eq. (6), that the range of product ion kinetic energies lies well outside the range for first-order or second-order focusing on single and dual-stage reflectrons, respectively. One solution is to extract and accelerate the ions orthogonally into a reflectron mass analyzer as suggested by Schey et al. [8].

The most common approach, however, has been to carry out the collisions at a lower energy (in the laboratory frame) and then raise the kinetic energy of the product ions before they enter the reflectron. In this way the range of kinetic energies presented to the reflectron will be:

$$E_b = \frac{m_b}{m_a} eV_c + eV_p \quad (7)$$

where eV_c is the laboratory collision energy and eV_p is the additional kinetic energy from post-collision acceleration of the ions. If $V_c \ll V_p$ then the product ions will be focused by a reflectron whose voltage V_R is slightly greater than $V_c + V_p$. In a 1992 instrument described by Boesl et al. [9] the first TOF stage was a linear drift region focused to the *space-focus plane* (the distance from the ion source at which ions formed in different locations converge), where the precursor ions are then mass-selected. The product ions were then reaccelerated into a reflectron.

This can also be accomplished by simply floating the collision cell to higher voltage. This decelerates the precursor ions prior to dissociation, and then reaccelerates the product ions. In 1993 two very similar instruments were reported, both using reflectrons in both MS stages, that is: an RTOF/RTOF configuration (Table 1). In the instrument described by Seeterlin et al. [10], precursor ions were fragmented after deceleration by photodissociation with an ArF excimer laser, and then reaccelerated before entering the second reflectron. Cotter and Cornish described instruments with a floatable collision cell located between two dual-stage [11] and two single-stage [12] reflectrons. They noted that product ion focusing decreased with the increase in mass difference from the precursor ion. They subsequently modified this instrument with a non-linear reflectron in the second stage (Fig. 3). The voltage law, which corresponded to an arc of a circle, was derived empirically based upon its focusing properties. The reflectron was subsequently called the *curved-field reflectron* [2]. More recently, as we have noted, a quadratic reflectron has been employed as MS2 in an instrument developed by Giannakopoulos et al. [6] in a TOF/RTOF configuration.

3. Commercial TOF/TOF mass spectrometers

Similar approaches are used on commercial tandem instruments. For example, the Applied BioSystems (Framingham, MA, USA) model 4700 and 4800 TOF/TOF mass spectrometers decelerate the precursor ions from 20 keV to 1–2 keV using

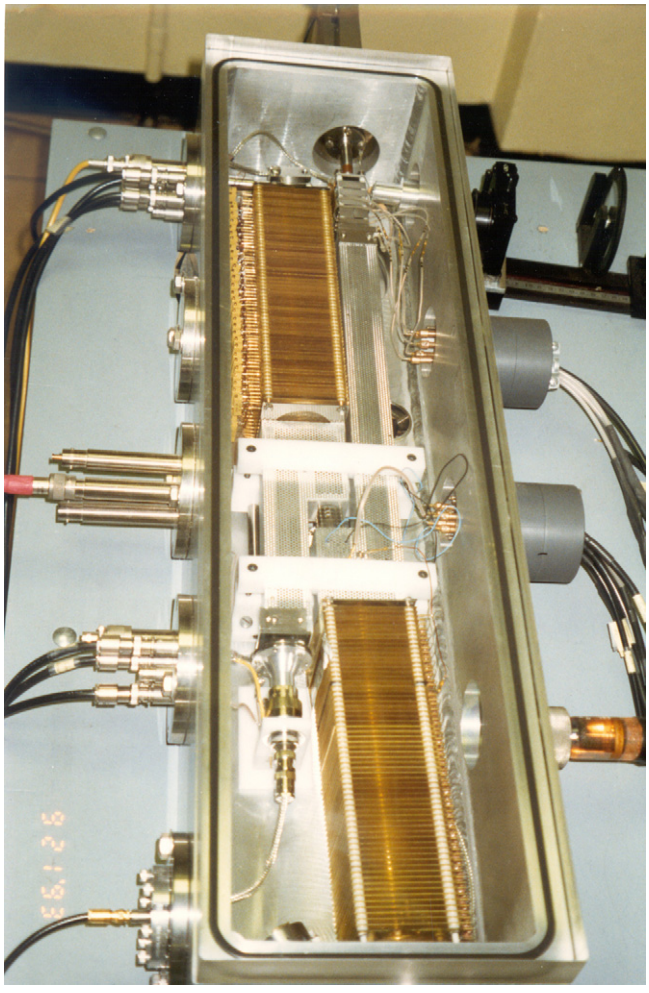

Fig. 3. The tandem RTOF/RTOF instrument which introduced the curved-field reflectron.

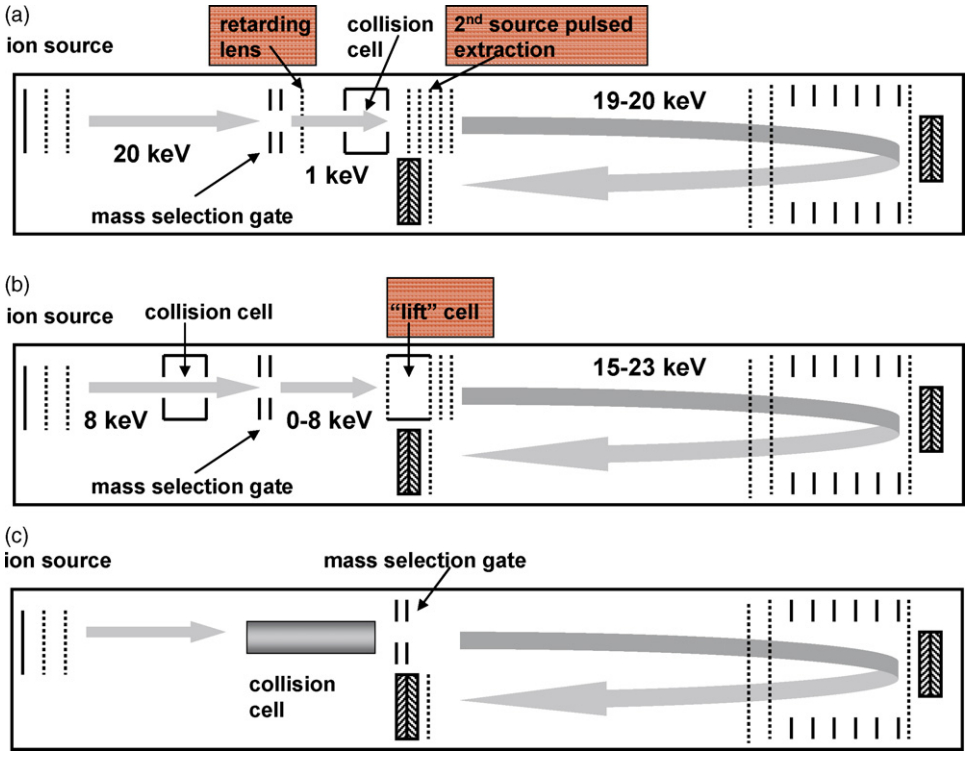

Fig. 4. Simplified schematic comparison of tandem TOF/TOF instruments: (a) Applied BioSystems, (b) Bruker Daltonics and (c) modified Kratos AXIMA CFR.

a series of retarding lenses (Fig. 4a). The precursor ions are mass selected by a *timed ion selector* (TIS), composed of a dual deflector gating system [13], and then dissociated in a collision chamber floating at 18 kV. The product ions enter a second source where they are reaccelerated (toward ground) and refocused by pulsed extraction [13,14]. The product ions thus have a relatively narrow energy spread (1 or 2 keV) relative to the precursor energy, and are therefore easily focused by the reflectron. However, this scheme does limit the collision energies to 1 or 2 keV.

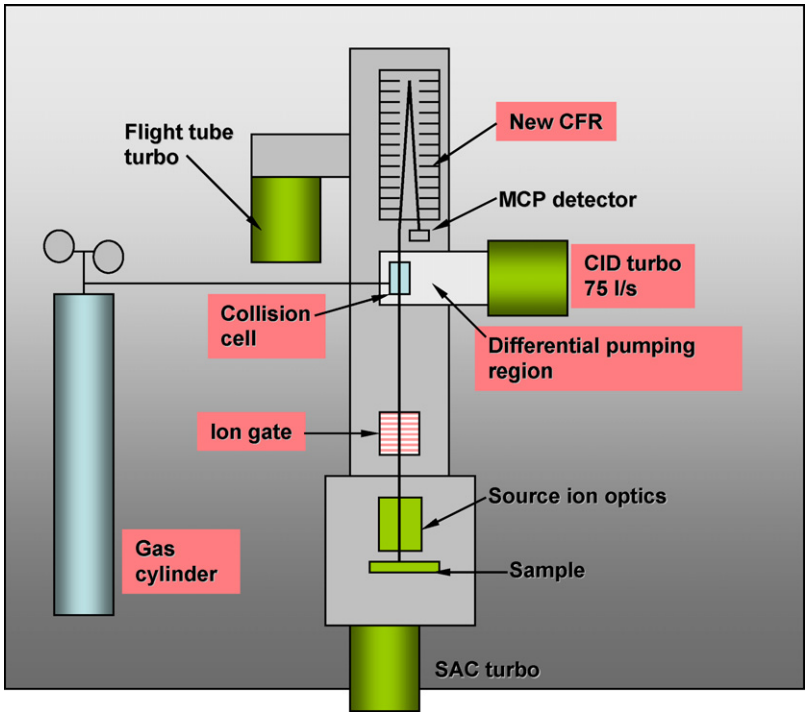

Fig. 5. Schematic of the tandem, curved-field reflectron mass spectrometer developed by Shimadzu.

In the Bruker Daltonics (Billerica, MA, USA) Ultraflex instrument the 8 keV precursor ions are not decelerated, so that collision energies in the laboratory frame are 8 keV (Fig. 4b). (In this case, ions are selected by a TIS that has a short (nanosecond) settling time at ground potential while switching from positive to negative deflection to eliminate effects of fringing fields on the resolving power.) After dissociation, the product ions enter a lift cell which sends them into the reflectron with an energy range of 17–25 keV [15].

Using a similar TOF/RTOF configuration, our laboratory more recently developed a tandem TOF mass spectrometer by modifying a Kratos (Manchester, UK) AXIMA CFR (Fig. 4c) with the addition of a collision chamber [16]. Because the curved-field reflectron was used, it was not necessary to decelerate the precursor ions, or to reaccelerate (or "lift") the product ions. As a result, the collision energies are 20 keV. A commercial version of this instrument has been developed by the Shimadzu Corporation (Kyoto, Japan) but includes some important differences [17]. In the AXIMA TOF^2 the collision cell is located after the mass selection gate and close to the curved-field reflectron to minimize losses from low angle scattering (Fig. 5). In addition, differential pumping reduces transmission losses from collisions outside the collision chamber. Both the AXIMA CFR and TOF^2 instruments were used in the applications that follow.

4. Characteristics of the curved-field reflectron

In the MS mode the curved-field reflectron produces essentially the same high mass resolution available on single and dual-stage reflectron instruments. In particular, both of the AXIMA instruments used in this work have a mass resolution up to 20,000 at m/z 5000. In the MS mode mass calibration is not effected by the non-linear field, as it always follows a square-root law in any linear or reflectron instrument, and mass accuracy is generally below 5 ppm. In the MS/MS mode mass selection in the AXIMA CFR is about 1/70, while in the TOF^2 a dual Bradbury–Nielsen gating system improves this to 1/400 or about ±1 Da at m/z 1000. Also in the MS/MS mode, mass calibration does not follow the linear law common for single-stage reflectrons, i.e. the $4(m_b/m_a)d$ term in the equation:

$$t_b = \left(\frac{m_a}{2eV}\right)^{1/2}\left[L_1 + L_2 + 4\frac{m_b}{m_a}d\right]$$

Instead, the product ion spectrum is calibrated empirically using a calibration compound such as $Pro_{15}Arg$, which provides a complete set of y-series ions [2]. This calibration is done only once, as it calibrates the ratios between product and precursor ion masses.

The curved-field reflectron has been used on instruments that were not tandems, to obtain product ion mass spectra from metastable fragmentation, a method generally known as *post-source decay* or PSD [18]. When carried out using single and dual-stage reflectrons the acquisition of PSD mass spectra required stepping the reflectron voltage, a cumbersome procedure that was not required for the CFR which focused all product ions simultaneously [2]. Because PSD has been associated with that particular procedure, it has been common to return to the more traditional term of *metastable fragmentation* to describe the processes occurring in tandem TOF instruments in the absence of a collision gas. That is the case as well for both the AXIMA CFR and TOF^2 instruments used here, both of which have distinct first and second mass analyzers, but differ in the absence or presence, respectively, of a collision chamber.

In a tandem time-of-flight then, the CFR offers two very specific advantages. The first is the ability to carry out very high energy collisions. The second is that all metastable fragmentation is recorded, along with any collision induced fragmentation, on the same mass scale. Because the CFR instrument does not require *metastable suppression*, there is the potential for improved sensitivity in the MS/MS mode. At the same time, slight differences in kinetic energies between metastable products and those formed after a collision with helium will produce differences in flight times in the linear

Table 2
Peptides observed in the tryptic digest of cleaved cystatin C

Residues	Observed MW	Sequence	MS/MS?
1–8	825.00	SSPGKPPR	
9–25	1800.91	LVGGPMDASVEEEGVRR	Yes
9–25	1816.94	LVGGPMDASVEEEGVRR oxidation (M)	Yes
25–36	1382.76	RALDFAVGEYNK	
36–36	1226.68	ALDFAVGEYNK	Yes
46–45	2303.93	ALDFAVGEYNKASNDMYHSR oxidation (H)	Yes
37–45	1080.54	ASNDMYHSR	
37–45	1096.55	ASNDMYHSR oxidation (HW)	
46–53	912.62	ALQVVRAR	
76–92	2060.92	TQPNLDNCPFHDQPHLK (carbamidomethyl)	Yes

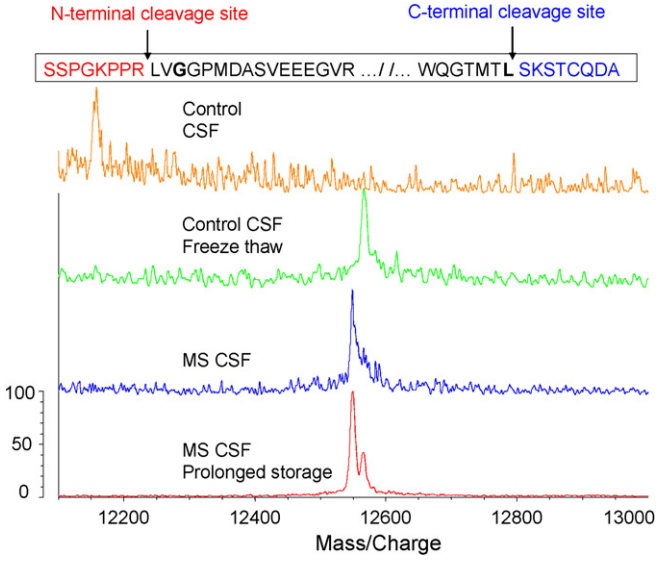

Fig. 6. A portion of the SELDI mass spectra of CSF samples showing the N-terminal and C-terminal cleavage products obtained on the AXIMA CFR.

Table 3
Peptides observed in the tryptic digest of histone ascetyltransferase

Number	Residues	Mass	Peptide sequence	Number	Residues	Mass	Peptide sequence
1	2–10	1073.0	**GSSHHHHHH**	36	238–256	2313.0	**ELPYFEGDFWPNVLEESIK**
2	2–14	1433.3	**GSSHHHHHHSSGE**	37	248–256	1029.2	**PNVLEESIK**
3	2–16	1661.7	**GSSHHHHHHSSGNL**	38	257–265	1191.2	**ELEQEEEER**
4	2–17	1824.0	**GSSHHHHHHSSGNLY**	39	266–281	1838.2	**KREENTSNESTDVTK$_{Ac}$G**
5	2–18	1971.7	**GSSHHHHHHSSGNLYF**	40	266–284	2168.6	**KREENTSNESTDVTK$_{Ac}$GDSK**
6	16–28	1497.7	**LYFGGHKENKFSA**	41	266–285	2324.3	**KREENTSNESTDVTK$_{Ac}$GDSK$_{Ac}$N**
7	30–35	729.8	**RLPSTR**	42	266–286	2396.9	**KREENTSNESTDVTK$_{Ac}$GDSK$_{Ac}$NA**
8	36–43	951.4	**LGTFLENR**	43	266–287	2566.6	**KREENTSNESTDVTK$_{Ac}$GDSK$_{Ac}$NAK$_{Ac}$**
9	44–49	764.4	**VNDFLR**	44	266–268	2694.9	**KREENTSNESTDVTK$_{Ac}$GDSK$_{Ac}$NAK$_{Ac}$K**
10	50–55	780.1	**RQNHPE**	45	266–289	2864.4	**KREENTSNESTDVTK$_{Ac}$GDSK$_{Ac}$NAK$_{Ac}$K$_{Ac}$K**
11	50–62	1508.9	**RQNHPESGEVTVR**	46	266–289	2907.9	**KREENTSNESTDVTK$_{Ac}$GDSK$_{Ac}$NAK$_{Ac}$K$_{Ac}$K$_{Ac}$**
12	51–62	1363.9	**QNHPESGEVTVR**	47	266–290	3020.7	**KREENTSNESTDVTK$_{Ac}$GDSK$_{Ac}$NAK$_{Ac}$K$_{Ac}$K$_{Ac}$N**
13	61–72	1338.9	**VRVVHASDKTVE**	48	266–291	3135.2	**KREENTSNESTDVTK$_{Ac}$GDSK$_{Ac}$NAK$_{Ac}$K$_{Ac}$K$_{Ac}$NN**
14	70–78	989.4	**TVEVKPGMK**	49	266–292	3263.2	**KREENTSNESTDVTK$_{Ac}$GDSK$_{Ac}$NAK$_{Ac}$K$_{Ac}$K$_{Ac}$NNK**
15	70–80	1260.5	**TVEVK$_{Ac}$PGMKAR**	50	266–292	3305.2	**KREENTSNESTDVTK$_{Ac}$GDSK$_{Ac}$NAK$_{Ac}$K$_{Ac}$K$_{Ac}$NNK$_{Ac}$**
16	81–94	1634.7	**FDVSGEMAESFPYR**	51	266–293	3433.3	**KREENTSNESTDVTK$_{Ac}$GDSK$_{Ac}$NAK$_{Ac}$K$_{Ac}$K$_{Ac}$NNK$_{Ac}$K**
17	97–129	3732.3	**ALFAFEEIGDVDLCFFGMHVQEYGSDCPPPNQR**	52	266–293	3475.5	**KREENTSNESTDVTK$_{Ac}$GDSK$_{Ac}$NAK$_{Ac}$K$_{Ac}$K$_{Ac}$NNK$_{Ac}$K$_{Ac}$**
18	131–141	1344.2	**VYISYLDSVHF**	53	266–294	3576.2	**KREENTSNESTDVTK$_{Ac}$GDSK$_{Ac}$NAK$_{Ac}$K$_{Ac}$K$_{Ac}$NNK$_{Ac}$K$_{Ac}$T**
19	131–145	1872.5	**VYISYLDSVHFFRPK**	54	266–295	3663.4	**KREENTSNESTDVTK$_{Ac}$GDSK$_{Ac}$NAK$_{Ac}$K$_{Ac}$K$_{Ac}$NNK$_{Ac}$K$_{Ac}$TS**
20	136–145	1247.8	**LDSVHFFRPK**	55	266–296	3791.9	**KREENTSNESTDVTK$_{Ac}$GDSK$_{Ac}$NAK$_{Ac}$K$_{Ac}$K$_{Ac}$NNK$_{Ac}$K$_{Ac}$TSK**
21	141–145	695.0	**FFRPK**	56	266–296	3834.2	**KREENTSNESTDVTK$_{Ac}$GDSK$_{Ac}$NAK$_{Ac}$K$_{Ac}$K$_{Ac}$NNK$_{Ac}$K$_{Ac}$TSK$_{Ac}$**
22	149–164	1912.3	**TAVYHEILIGYLEVK**	57	266–297	3947.5	**KREENTSNESTDVTK$_{Ac}$GDSK$_{Ac}$NAK$_{Ac}$K$_{Ac}$K$_{Ac}$NNK$_{Ac}$K$_{Ac}$TSK$_{Ac}$N**
23	155–163	1084.3	**ILIGYLEYV**	58	266–298	4077.4	**KREENTSNESTDVTK$_{Ac}$GDSK$_{Ac}$NAK$_{Ac}$K$_{Ac}$K$_{Ac}$NNK$_{Ac}$K$_{Ac}$TSK$_{Ac}$NK**
24	157–164	985.2	**IGYLEYVK**	59	266–298	4118.3	**KREENTSNESTDVTK$_{Ac}$GDSK$_{Ac}$NAK$_{Ac}$K$_{Ac}$K$_{Ac}$NNK$_{Ac}$K$_{Ac}$TSK$_{Ac}$NK$_{Ac}$**
25	166–194	3287.5	**LGYTTGHIWACPPSEGDDYIFHCHPPDQK**	60	266–299	4205.1	**KREENTSNESTDVTK$_{Ac}$GDSK$_{Ac}$NAK$_{Ac}$K$_{Ac}$K$_{Ac}$NNK$_{Ac}$K$_{Ac}$TSK$_{Ac}$NK$_{Ac}$S**
26	169–194	2952.2	**TTGHIWACPPSEGDDYIFHCHPPDQK**	61	267–289	2736.8	**REENTSNESTDVTK$_{Ac}$GDSK$_{Ac}$NAK$_{Ac}$K$_{Ac}$K$_{Ac}$**
27	186–197	1448.5	FHCHPPDQKIPK	62	285–293	1114.5	**NAKKKNNK$_{Ac}$K**
28	195–206	1558.6	IPKPKRLQEWYK	63	308–321	1515.7	KPGMPNVSNDLSQK
29	200–206	1022.8	**RLQEWYK**	64	308–328	2351.1	**KPGMPNVSNDLSQKLYATMEK**
30	201–206	867.0	**LQEWYK**	65	331–337	910.2	**EVFFVIR**
31	201–216	2027.4	LQEWYKKMLDKAVSER	66	338–365	2872.9	**LIAGPAANSLPPIVDPDPLIPCDLMDGR**
32	205–213	1139.9	YKKMLDK$_{Ac}$AV	67	366–373	907.3	**DAFLTLAR**
33	212–226	1823.9	AVSERIVHDYKDIFK	68	374–383	1232.9	**DKHLEFSSLR**
34	217–222	775.5	**IVHDYK**	69	374–383	1275.5	**DK$_{Ac}$HLEFSSLR**
35	233–258	2856.5	**LTSAK$_{Ac}$ELPYFEGDFWPNVLEESIK**	70	376–383	989.6	**HLEFSSLR**

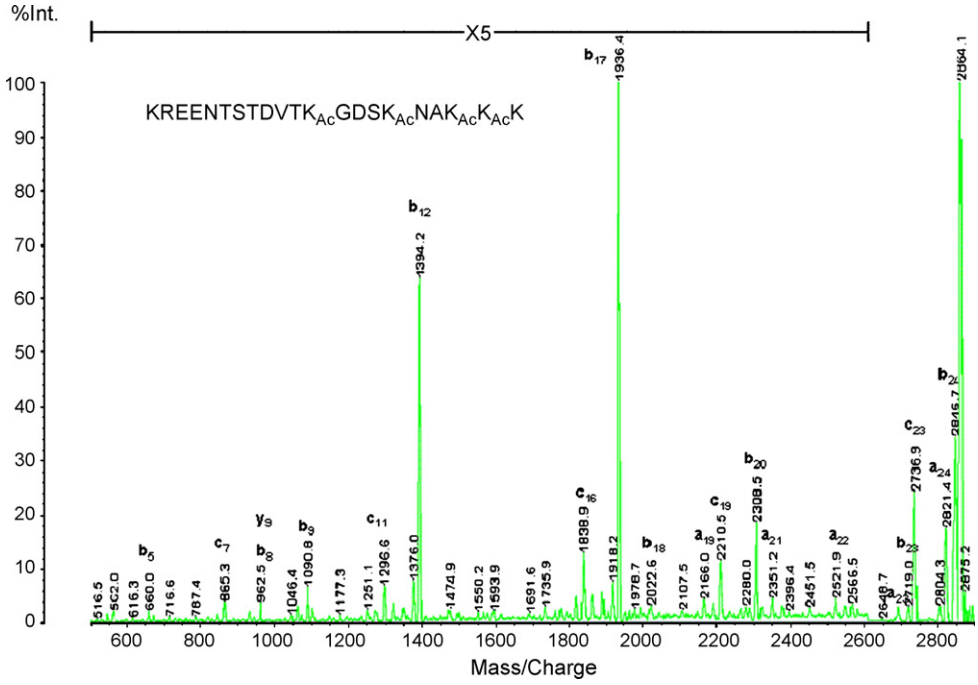

Fig. 7. MS/MS (metastable) spectrum of a tryptic peptide from p300 histone acetyltransferase having four acetylated lysine sites.

regions and can result in some degradation in product ion mass resolution and accuracy. In a tandem with a CFR, location of the collision cell well after the mass selection gate and close to the reflectron field is possible, and minimizes this problem as does (in any instrument) a reduction of the initial laser power that enhances the formation of metastable products.

5. Biomarker discovery: the cleavage of cystatin C and multiple sclerosis

Our laboratories have initiated several *neuroproteomics* studies that combine *surface-enhanced laser desorption/ionization* (SELDI) with high performance time-of-flight mass spectrometry to enable identification and detailed structural

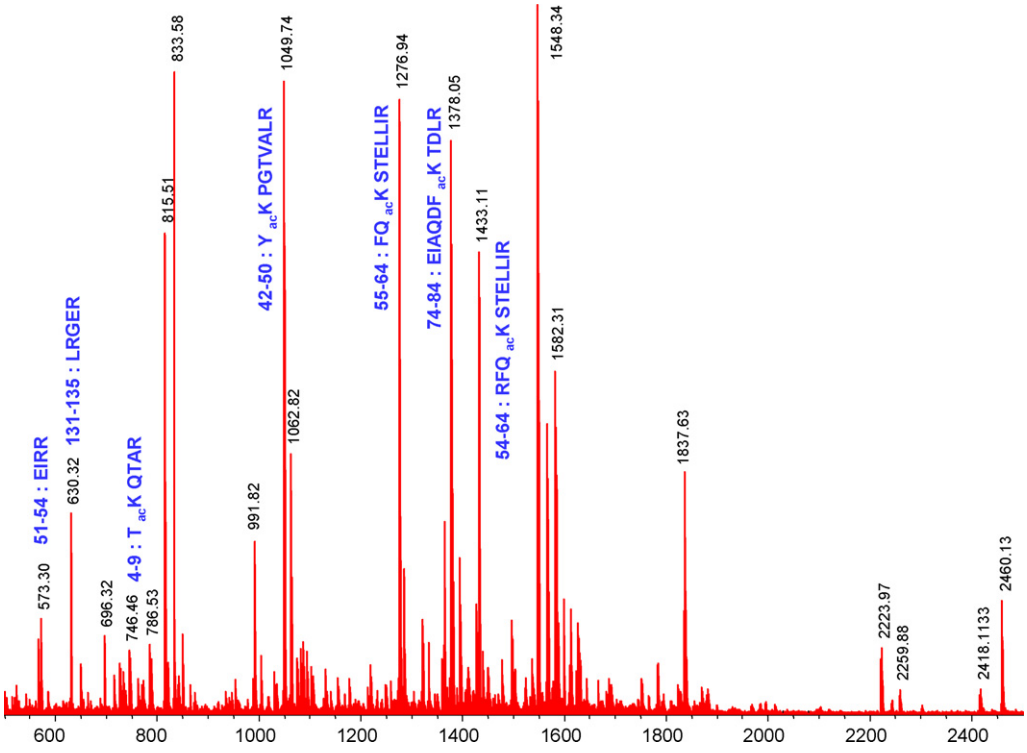

Fig. 8. MALDI mass spectrum of the tryptic digest of deuteroacetylated yeast histone H3.

characterization of potential protein biomarkers in the cerebral spinal fluid. Recently we reported that the differential expression of two proteins at 12.5 and 13.4 kDa corresponded to the cleavage of the eight C-terminal amino acids in cystatin C in patients with remitting relapse multiple sclerosis [19]. SELDI analysis of the tryptic digest of both proteins was carried out on a Kratos AXIMA CFR mass spectrometer, with both species identified as cystatin C by *protein mass fingerprinting*, while observation of the N-terminal tryptic fragment from the cleavage product confirmed the loss of the C-terminal residues. Additionally, MALDI MS/MS spectra obtained on the same instrument was used to confirm the amino acid sequences of the tryptic fragments (Table 2).

In more recent work we examined the effects of storage and freeze/thaw cycles, which result in cleavage of the eight N-terminal amino acids of cystatin C and a loss in its effect on cathepsin B activity [20]. The effect of one or more freeze/thaw cycles was a peptide with a measured mass of 12,543 Da, compared with the mass of 12,528 Da determined for the product associated with RRMS (Fig. 6). In addition, the effect of freeze/thaw cycles on a CSF sample obtained from a patient with RRMS revealed both cleavage products that were distinguishable by their masses.

The CSF has considerable potential as a proteome source for neurologically related diseases. Currently our laboratory is utilizing the *neuroproteome* in studies of aenemia and HIV, as

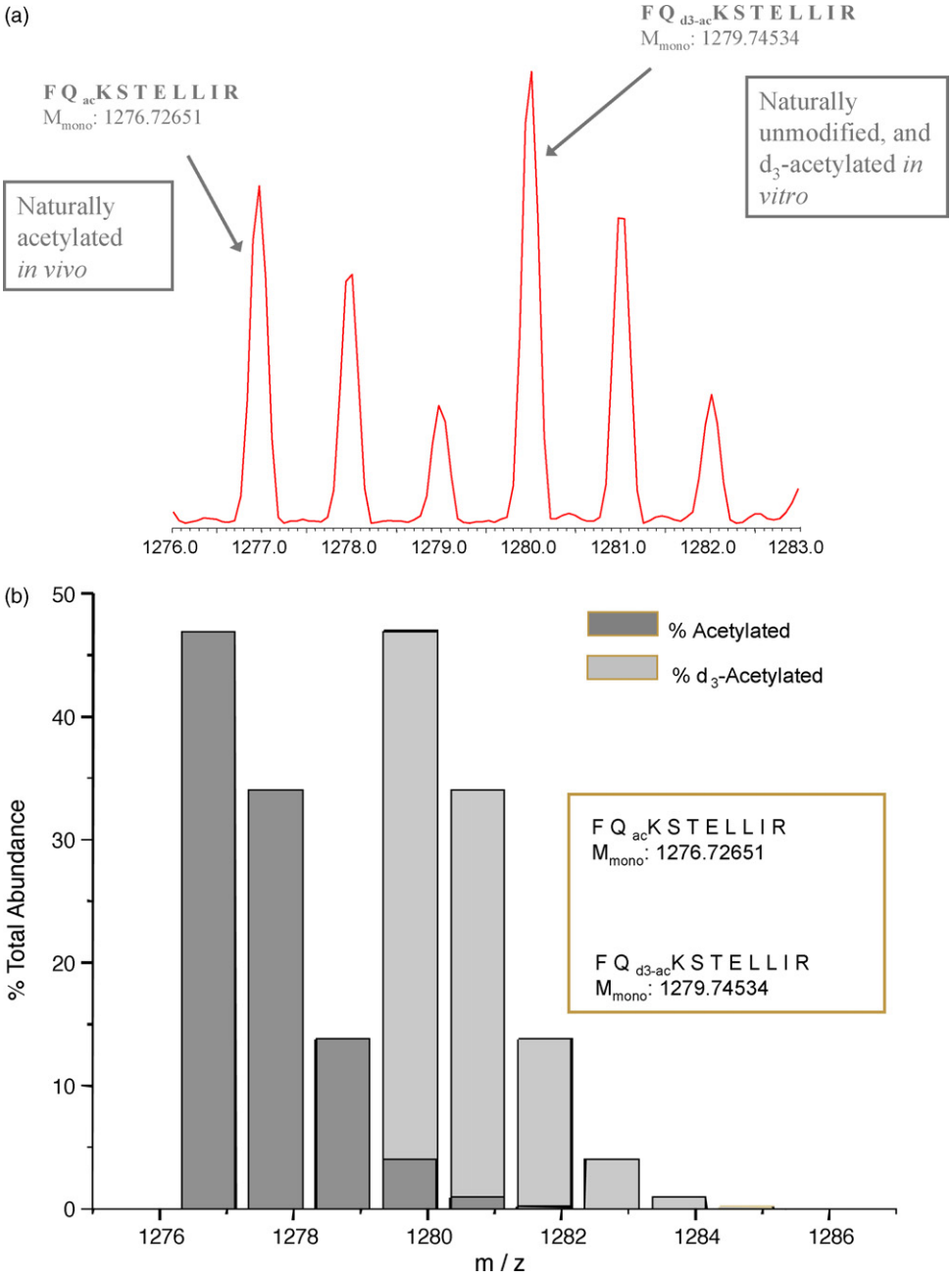

Fig. 9. (a) Expansion of the tryptic digest mass spectral region containing the K_{56} site. (b) Scheme showing the method of calculation of the percentage of acetylated sites.

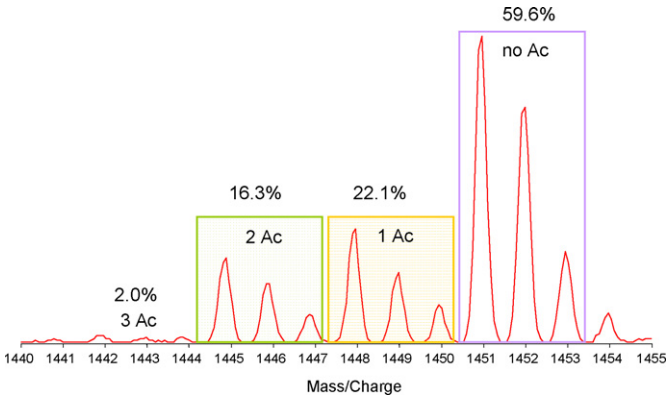

Fig. 10. Expansion of the mass spectra of a partially acetylated, and subsequently deutero-acetylated, histone H4 containing four lysine residues.

well as multiple sclerosis. While a somewhat simpler proteome than that derived from blood, CSF nonetheless poses particular challenges in collection, storage and sample handling.

6. Acetylation of histones and HATs

The nucleosome complex consists of approximately 145–147 DNA base pairs wrapped around a nucleosome core composed of two copies each of the histones H2A, H2B, H3 and H4 arranged as an octamer. The reversible acetylation and deacetylation of histones and other DNA-binding proteins is a key mechanism in regulating gene transcription. *Histone acetyltransferases* (HATs) can covalently modify histones and other substrates by transferring acetyl groups from acetyl-CoA to the ε-amino groups of specific lysine residues within the proteins. The cellular 300 kDa protein p300 and its close homolog CBP (cAMP response element-binding protein-binding protein), often referred to as p300/CBP, are highly conserved global transcriptional coactivators and histone acetytransferases in higher eukaryotes. By acetylating histones as well as a number of non-histone proteins, p300/CBP play key roles in a variety of transcriptional pathways, including cellular proliferation, differentiation and apoptosis. Recently, we used tandem TOF mass spectrometry to characterize the acetylation, probably through self-catalysis, within a purified recombinant HAT domain of p300 protein [21,22]. The analyses were carried out on the Kratos AXIMA CFR without collision gas.

The p300 protein was digested with trypsin, with only partial cleavages occurring at the acetylated lysine residues. Thus, a number of the resultant peptides contained multiple acetylation sites. Fig. 7 shows the MS/MS spectrum of a peptide containing four acetylated lysine residues, which can be identified from the masses of the amino acid sequence ions. Though the analysis was carried out without collision gas, that is utilizing metastable or laser-induced dissociation alone, sequence coverage by MS/MS is very high (Table 3). Of the 70 peptides observed in the initial MS spectra of the fractionated mixture, all but 6 of these yielded an MS/MS spectrum.

7. Site-specific quantitation using isotope labeling and TOF^2 mass spectrometry

The histones themselves can be hyper-acetylated, mono-, di and tri-methylated and ubiquitylated at lysine residues, and phosphorylated at serine/threonine residues, primarily in the so-called “tail regions”. We have developed an approach for

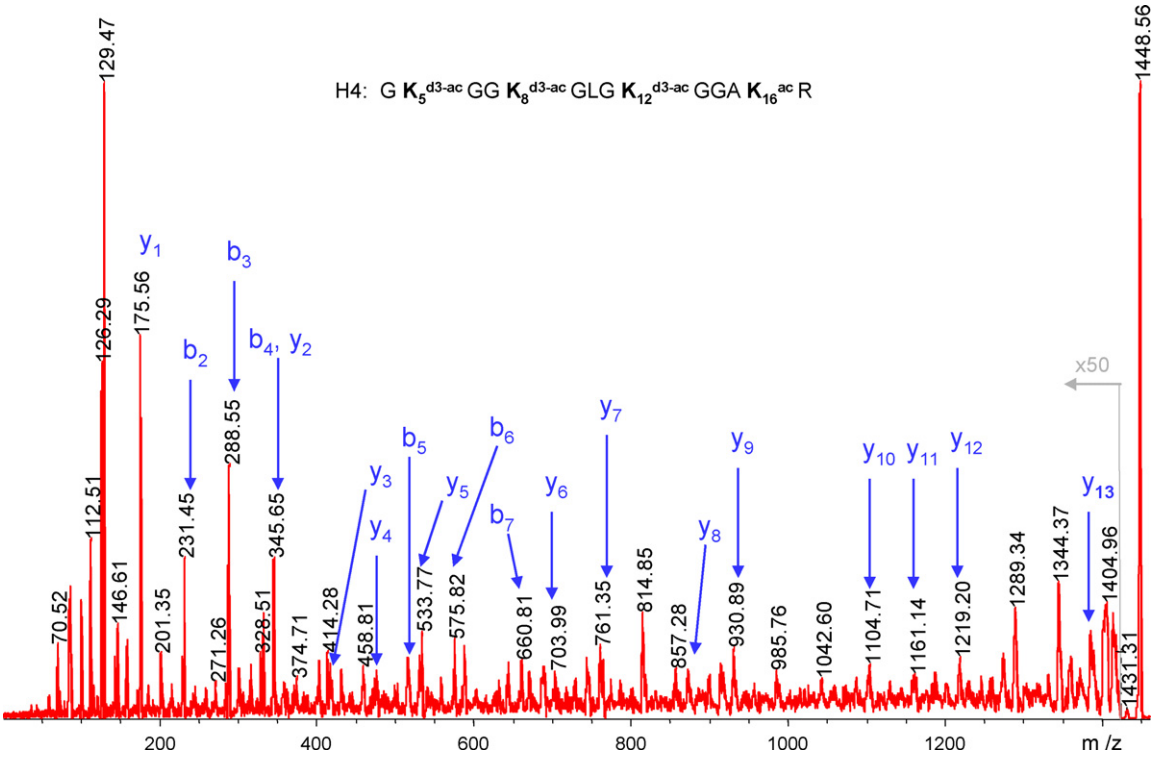

Fig. 11. MS/MS (CID) spectrum of the d_9 analog corresponding to the mono-acetylated yeast histone H4.

determining quantitatively the extent of acetylation at each site by deutero-acetylating all of the unmodified lysines and then comparing the mass spectral intensities of the d_0 and d_3 analogs of the tryptic peptides [23]. Specifically, intact partially acetylated yeast histone H3 was reacted with deuterated acetic anhydride prior to digestion with trypsin. Digestion of the now fully acetylated protein resulted in cleavage almost exclusively at arginine residues. Fig. 8 shows a mass spectrum of the H3 digest. For those peptides containing a lysine residue, both the d_0 and d_3 acetylated peptide peaks are observed. Expansion of the mass spectrum for the peptide containing lysine-56 (Fig. 9) enables calculation of the percent acetylation (the d_0 analog) of 45%.

The need for efficient tandem mass spectrometry occurs for those peptides containing multiple sites, and provides the opportunity to determine how acetylated isoforms are distributed and perhaps in what order acetylation occurs. Fig. 10 shows the mass spectrum of the molecular ion region for a deuteroacetylated tryptic peptide from yeast histone H4 containing four lysine residues. The observed d_0, d_3, d_6, d_9 and d_{12} analogs correspond to acetylation at all four, three, two, one and no sites, respectively. The MS spectrum shows that 59.6% of these peptides were not originally acetylated, while 22.1 and 16.3% were mono- and di-acetylated, respectively. Tandem mass spectrometry is then used to determine (for example) whether a single acetylation occurs at one or more sites. Fig. 11 shows the high energy CID tandem mass spectrum of the mono-acetylated species, obtained on the AXIMA TOF^2 mass spectrometer. The masses observed are consistent with acetylation only on the K_{16} site. Similarly, it can also be shown that the peptides containing two acetylated lysines are acetylated only on the K_8 and K_{16} sites.

8. Conclusions and prospects

Interestingly, most of the current tandem and hybrid instruments using *collision-induced dissociation* (CID) employ *low energy* collisions. The boundary between low and high energies (in the laboratory scale) is certainly unclear and does depend upon the relative masses of the precursor ion and the target gas. However, the low energy CID process does involve repetitive collisions that raise the internal energy uniformly and in steps, leading to cleavage of the weakest bond. This has generally been implicated in the often observed losses of post-translational modification groups (particularly phosphate and carbohydrate) from peptides. High energy CID, on the other hand, generally involves single collisions, and is commonly used on sector and TOF instruments. The tandem TOF instrument described here, which uniquely utilizes a curved-field reflectron, provides considerably higher collision energy (20 keV) than the 1–2 and 8 keV energies used in other instruments. High energy collisions may provide fragmentation that is more randomized and may enable better observation of the location of post-translational modifications. What will be tested in upcoming work is the degree to which very high energies provides an analytical advantage.

Acknowledgements

The development of the tandem mass spectrometer and its applications to many biological projects has involve a number of individuals who should be acknowledged. In particular, we acknowledge Timothy Cornish as the co-inventor of the curved-field reflectron, and Sergei Ilchenko, Robert English and Ben Gardner for the development of the tandem TOF. The studies on cystatin C were a collaboration with Avindra Nath in the Department of Neurology at the Johns Hopkins School of Medicine and were carried out by Rebekah Gundry and Christine Jelinek in the Cotter Lab; David Wheeler, Caroline Anderson, David Irani and Peter Calabresi in Neurology; and Stacey Moore from Ciphergen BioSystems (Freemont, CA, USA). Mass spectral determination of the acetylation sites of histone acetyl transferase was a collaborative project with Philip Cole and Paul Thompson in the Department of Pharmacology and carried out by Dongxia Wang. Quantitative acetylation analysis was a collaboration with Alain Verreault from the University of Montreal and Jef Boeke from the Johns Hopkins High Throughput Biology Center; and carried out by Ivana Celic and Wendell Griffith.

This work was carried out at the Middle Atlantic Mass Spectrometry Laboratory at the Johns Hopkins School of Medicine and supported in part by a contract (N01 HV28180) to J. VanEyk from the National Heart, Lung and Blood institute, a grant (GM/RR64402) from NIH to R.J. Cotter and a grant (U54 RR020839) to Jef Boeke.

References

[1] Mass Spec Terms Project, IUPAC Analytical Chemistry Division (Division V), http://www.msterms.com/wiki.
[2] T.J. Cornish, R.J. Cotter, Rapid Commun. Mass Spectrom. 7 (1993) 1037.
[3] B.A. Mamyrin, V.I. Karataev, D.V. Shmikk, V.A. Zagulin, Sov. Phys. JETP 37 (1973) 45.
[4] R.J. Cotter, Time-of-Flight Mass Spectrometry: Instrumentation and Applications in Biological Research, American Chemical Society, Washington, DC, 1997.
[5] B.A. Mamyrin, Int. J. Mass Spectrom. Ion Processes 131 (1994) 1.
[6] A.E. Giannakopoulos, B. Thomas, A.W. Colburn, D.J. Reynolds, E.N. Raptakis, A.A. Makarov, P.J. Derrick, Rev. Sci. Instrum. 73 (2002) 2115.
[7] D.T. Jardine, J. Morgan, D.S. Alderdice, P.J. Derrick, Org. Mass Spectrom. 27 (1992) 1077.
[8] K.L. Schey, R.G. Cooks, A. Kraft, R. Grix, H. Wollnik, Int. J. Mass Spectrom. Ion Processes 94 (1989) 1.
[9] U. Boesl, R. Weinkauf, E.W. Schlag, Int. J. Mass Spectrom. Ion Processes 112 (1992) 121.
[10] M.A. Seeterlin, P.R. Vlasak, D.J. Beussman, R.D. McLane, C.G. Enke, J. Am. Soc. Mass Spectrom. 4 (1993) 751.
[11] R.J. Cotter, T.J. Cornish, Anal. Chem. 65 (1993) 1043.
[12] T.J. Cornish, R.J. Cotter, Org. Mass Spectrom. 28 (1993) 1129.
[13] K.F. Medzihradszky, J.M. Campbell, M.A. Baldwin, A.M. Falik, P. Juhasz, M.L. Vestal, A.L. Burlingame, Anal. Chem. 72 (2000) 552.
[14] A.L. Yergey, J.R. Coorssen, P.S. Backlund Jr., P.S. Blank, G.A. Humphrey, J. Zimmerberg, J.M. Campbell, M.L. Vestal, J. Am. Soc. Mass Spectrom. 13 (2002) 784.
[15] D. Suckau, A. Resemann, M. Schuerenberg, P. Hufnagel, J. Franzen, A. Holle, J. Anal. Bioanal. Chem. 376 (2003) 1618.
[16] R.J. Cotter, B. Gardner, S. Iltchenko, R.D. English, Anal. Chem. 76 (2004) 1976.
[17] E. Pittenauer, M. Zehl, O. Belgacem, E. Raptakis, R. Mistrik, G. Allmaier, J. Mass Spectrom. 41 (2006) 421.

[18] R. Kaufmann, P. Chaurand, D. Kirsch, B. Spengler, Rapid Commun. Mass Spectrom. 10 (1996) 1199.
[19] D.N. Irani, C. Anderson, R. Gundry, R.J. Cotter, S. Moore, D.A. Kerr, J.C. McArthur, N. Sacktor, C.A. Pardo, M. Jones, P.A. Calabresi, A. Nath, Ann. Neurol. 59 (2006) 237.
[20] D. Wheeler, C. Jelinek, C. Anderson, R. Gundry, D. Irani, P. Calabresi, R. Cotter, A. Nath, Ann. Neurol., in press.
[21] P. Thompson, D. Wang, L. Wang, M. Fulco, N. Pediconi, D. Zhang, W. An, Q. Ge, R.G. Roeder, J. Wong, M. Levrero, V. Sartorelli, R.J. Cotter, P.A. Cole, Nat.: Struct. Mol. Biol. 11 (2004) 308.
[22] D. Wang, P. Thompson, P.A. Cole, R.J. Cotter, Proteomics 5 (2005) 2288.
[23] I. Celic, H. Masumoto, W.P. Griffith, P. Meluh, R.J. Cotter, J.D. Boeke, A. Verreault, Curr. Biol. 16 (2006) 1280.